A Novel Tool for Breakdown Probability Predictions on Multi-Electrode Multi-Voltage Systems

Paolo Bettini[1,2], Nicola Pilan[2], and Ruben Specogna[3]

[1]Università di Padova, Dipartimento di Ingegneria Industriale, Padova 35131, Italy
[2]Consorzio RFX, EURATOM-ENEA Association, Padova 35127, Italy
[3]Università di Udine, Dipartimento di Ingegneria Elettrica, Gestionale e Meccanica, Udine 33100, Italy

An innovative approach for the voltage breakdown prediction in high-voltage systems, insulated by large vacuum gaps, is presented. It is based on the correlation between the clump mechanism and a statistical approach to the breakdown probability. The aim of this paper is twofold. First, the numerical solution of 3-D electrostatic problems by a couple of complementary formulations is presented. Second, an efficient post-processing tool is introduced, based on the analytical solution of the equations of motion in a domain covered by a tetrahedral mesh, to estimate the breakdown probability associated to the electrically charged microparticles leaving one electrode and clashing to the electrode with opposite polarity with sufficient energy to get vaporization. This approach has been benchmarked on a reference configuration (sphere/plane) problem and applied to calculate the particle trajectories in a very complex multi-electrode multi-voltage system.

***Index Terms*—Electrostatics, finite-element method, high voltage, ion beam.**

I. Introduction

ALTHOUGH the high vacuum is used extensively for the insulation of high-voltage devices in many research and industrial areas, no consolidated design criteria are available in the literature to predict the breakdown probability of a multi-electrode multi-voltage system, insulated by large vacuum gaps.

Nevertheless, an innovative approach for the voltage breakdown prediction of such complex systems has been formulated and validated against the experimental results [1]. It is based on the correlation between the clump mechanism [2], [3] and a statistical approach to the breakdown probability.

The evaluation of the breakdown voltage in terms of probability makes this model suitable for an engineering approach to the insulation design; in particular, the electrode profile design would be no longer based upon the electric field minimization, but upon the minimization of a new breakdown driver parameter.

The aim of this paper is twofold. First, the numerical solution of 3-D electrostatic problems by two complementary formulations is presented. Second, an efficient post-processing tool is introduced, based on the analytical solution of motion equations in a domain covered by a tetrahedral mesh. This tool is used to estimate the breakdown probability associated to the electrically charged microparticles leaving one electrode and clashing to the electrode with opposite polarity with sufficient energy to get vaporization.

The proposed approach is applied both to a reference bidimensional axisymmetric configuration (sphere/plane) and to a challenging 3-D multi-electrode multi-voltage system [the accelerator of ITERs neutral beam injector (NBI), see Fig. 1]. In [4], the electroquasi-static (EQS) behavior of crucial elements of the NBI system has been discussed. Here, we focus on the calculation of the electrostatic field configuration inside the beam accelerator.

Manuscript received June 29, 2013; revised August 3, 2013; accepted September 10, 2013. Date of current version February 21, 2014. Corresponding author: P. Bettini (e-mail: paolo.bettini@unipd.it).

Color versions of one or more of the figures in this paper are available online at http://ieeexplore.ieee.org.

Digital Object Identifier 10.1109/TMAG.2013.2281851

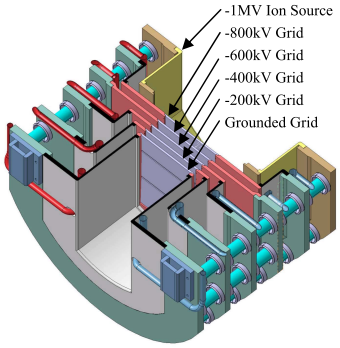

Fig. 1. Cutaway of ITER NBI accelerator. It is composed of five acceleration grids, biased at increasing voltages, with steps of 200 kV, from 0 V (ground level) up to −1 MV (ion source).

II. Microparticles Probabilistic Model

An electrostatic system is considered, which is composed by a number of electrodes polarized at different voltages (V_i). The breakdown probability associated to the macroscopic area A_i of the ith electrode can be expressed as

$$dp_i = n_i * dA_i \tag{1}$$

where n_i denotes the number of microparticles per unit area, which can be detached by electrostatic forces and impinge another electrode with sufficient energy to get vaporization.

Using the same approach followed by the failure analysis theory [5], the voltage holding probability R_H is

$$R_H = \prod_{i=1}^{M} (1 - p_i) \tag{2}$$

being M the overall number of electrode subdivisions. Then, the breakdown probability for the whole system is simply

$$P = 1 - R_H. \tag{3}$$

The crucial point is the identification of a relationship between n_i and the physical mechanism underlying the clump induced breakdown. According to Slivkov–Cranberg criterion [3], a breakdown can occur if the electric field at the

receiving electrode is sufficient to initiate a local Paschen discharge across the vapor bubble created by the clump impact

$$W = \Delta V\, E(P)\, E(Q)^{2/3} > W_S \tag{4}$$

where $E(P)$ denotes the norm of the electric field at starting point P (responsible for clump charging), $E(Q)$ denotes the norm of the electric field at destination point Q (responsible for the vapor bubble ionization), ΔV is the voltage between the two electrodes, and W_S is a threshold value.

The fundamental assumption is that the number of microparticles that potentially can produce a breakdown is a monotonic function of W. A functional dependence described by the Weibull's distribution is assumed

$$n(W) = \left(\frac{W}{W_0}\right)^m \tag{5}$$

where W_0 and m are the parameters depending mainly on material and surface treatments. W_0 is the reference value, which corresponds to $R_H = 1/e \approx 0.368$, for a couple of ideal plane parallel electrodes having an area $A = 1m^2$.

In this paper, the values of W_0 and m have been chosen according to the results of a dedicated experimental campaign, on stainless steel electrodes, carried out at high-voltage Padova test facility (HVPTF) [6]: $W_0 = 2.35e^{17}$ and $m = 20$.

III. Electrostatic Complementary Formulations

An efficient numerical code (CAFE) is used to solve electrostatic problems in 3-D, non-trivial domains. CAFE code combines the standard FEM formulation **V**, based on the electric scalar potential, with an original formulation **P** that employs the electric vector potential [7]. The advantage of using two formulations, arising from complementary potentials, is that the results of the two formulations may be used as a robust error estimator for adaptively refine the mesh and to have a reliable control on the accuracy of the solution [8]. Nonetheless, complementarity requires a complicated topological preprocessing [9] and that is why it is not widely used in practice.

The computational domain is covered by a tetrahedral mesh whose incidences are encoded in the *cell complex* $\mathcal{K}$ represented by the standard incidence matrices **G**, **C**, and **D**. A dual barycentric complex $\tilde{\mathcal{K}}$ is obtained from $\mathcal{K}$ using the *barycentric subdivision*. The matrices $\tilde{\mathbf{G}} = \mathbf{D}^T$, $\tilde{\mathbf{C}} = \mathbf{C}^T$ and $\tilde{\mathbf{D}} = -\mathbf{G}^T$ represent the incidence matrices of $\tilde{\mathcal{K}}$.

To formulate the problem using the vector potential formulation, an array of voltages $\tilde{\mathbf{U}}$ on dual edges $\tilde{e}$, an array of electric fluxes $\mathbf{\Phi}$ on faces f, and an electric vector potential **P** on edges e are introduced. The vector potential that in absence of source charges is defined through

$$\Psi = \mathbf{CP} + \sum_{i=1}^{N} Q_g^i\, \mathbf{\Pi}^i \tag{6}$$

verifies the discrete Gauss' law $\mathbf{D\Psi} = \mathbf{0}$, where $\{\mathbf{\Pi}^i\}_{i=1}^N$ is a set of thick links, $N+1$ is the number of electrodes, and $\{Q_g^i\}_{i=1}^N$ is the corresponding set of independent induced electric charges, one for each electrode but one that is chosen as a reference electrode.

Concerning boundary conditions (BCs), **P** is set to zero for all edges belonging the portion of $\partial\mathcal{K}$ subjected to homogeneous Neumann BCs. The constitutive matrix **H** relates the flux $\mathbf{\Psi}$ to voltage $\tilde{\mathbf{U}}$ with $\tilde{\mathbf{U}} = \mathbf{H}\,\mathbf{\Psi}$.

Concerning the construction of **H**, one can use the standard mass matrix of finite elements produced with face basis functions or piecewise-uniform face vector basis functions defined in [10].

By combining the Faraday's discrete law $\mathbf{C}^T\tilde{\mathbf{U}} = \mathbf{0}$ with (6) and the constitutive law, we obtain

$$\mathbf{C}^T\mathbf{HCP} + \sum_{j=1}^{N} \left(\mathbf{C}^T\mathbf{H\Pi}^j\right) Q_g^j = \mathbf{0}. \tag{7}$$

In addition, a set of non-local Faraday's laws [7] has to be written on each thick link as $\mathbf{\Pi}^{iT}\tilde{\mathbf{U}} = U_g^i,\ i \in \{1, \ldots, N\}$, where U_g^i is the desired voltage between the reference electrode and the ith electrode. The equation is expanded as

$$\left(\mathbf{\Pi}^{iT}\mathbf{HC}\right)\mathbf{P} + \sum_{j=1}^{N} \left(\mathbf{\Pi}^{iT}\mathbf{H\Pi}^j\right) Q_g^j = U_g^i. \tag{8}$$

The final algebraic linear system (sparse, symmetric, and singular) is iteratively solved without applying any gauge. Then, a dedicated post-processing tool is used to compute the particle trajectories neglecting the collisions.

IV. Calculation of Particle Trajectories

The evaluation of W, according to (4), would require the knowledge of the electric field only in the anodic/cathodic regions. Nevertheless, the electric field in the whole domain is needed to calculate the trajectory of each charged particle; obviously, this task can be carried out in a closed form only for almost useless geometries (e.g., parallel planes or coaxial cylinders).

In general, the knowledge of initial velocity $\bar{v}_0$, mass m, and electric charge q of the particle (clump) is also required. Nonetheless, in [1], it has been demonstrated that the trajectory of a clump, with constant charge q, depends only upon the geometry of the electrostatic system, under the hypothesis of nonrelativistic motion and initial condition $\bar{v}_0 = 0$.

A. Main Procedure

The proposed procedure relies on the idea to calculate the particle trajectory by moving through adjacent elements of $\mathcal{K}$, avoiding the standard integration of particle motion equations by a common Runge–Kutta (RK) scheme.

For this purpose, in the preprocessing phase, together with the standard incidence matrices, a *proximity* matrix is saved as well, which encodes for each tetrahedron the information on adjacent cells; as a special case, boundary faces are flagged with integers corresponding to the partitions of $\partial\mathcal{K}$, where Dirichlet or Neumann BCs are assigned.

The calculation of the ith trajectory starts from the barycenter $\mathbf{P_0}$ of the ith electrode subdivision, with initial condition $\bar{v}_0 = 0$. The procedure, which allows to calculate the trajectory inside each tetrahedron, is described in the following section. This procedure is applied to calculate the trajectory from $\mathbf{P_0}$ to $\mathbf{Q_0}$ (exit point of the first tetrahedron), and then repeated for all tetrahedra spanned along the motion, until the target electrode is reached.

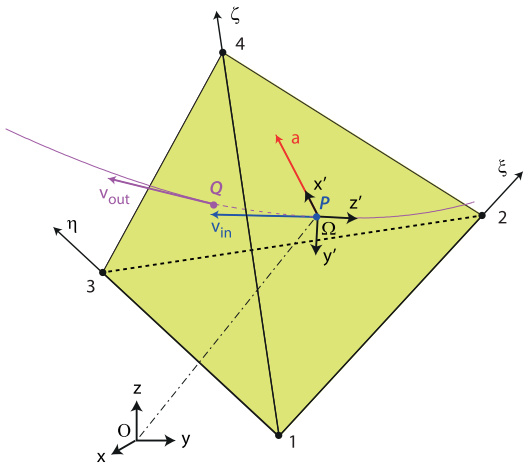

Fig. 2. Local coordinates (ξ, η, ζ) on a tetrahedron. Absolute (x, y, z) and local (x', y', z') Cartesian frames. **P** (**Q**) denotes the entry (exit) point of a charged particle with initial (final) velocity $\bar{v}_{\text{in}}$ ($\bar{v}_{\text{out}}$).

B. Analytical Solution Inside Each Tetrahedron

By adopting first-order elements, the electric field E inside a generic tetrahedron is uniform, and a charged particle is subjected to a uniformly accelerated motion (see Fig. 2). The acceleration $\bar{a}$ is constant along the direction of E, with initial velocity $\bar{v}_{\text{in}}$; the coordinates of the exit point **Q** and the corresponding velocity $\bar{v}_{\text{out}}$ can be calculated as described in the following.

To simplify the evaluation of the trajectories, local coordinates (ξ, η, ζ) are introduced through the affine mapping

$$\begin{bmatrix} x \\ y \\ z \end{bmatrix} = \begin{bmatrix} x_1 \\ y_1 \\ z_1 \end{bmatrix} + J \begin{bmatrix} \xi \\ \eta \\ \zeta \end{bmatrix} \tag{9}$$

being

$$J = \begin{bmatrix} x_2 - x_1 & x_3 - x_1 & x_4 - x_1 \\ y_2 - y_1 & y_3 - y_1 & y_4 - y_1 \\ z_2 - z_1 & z_3 - z_1 & z_4 - z_1 \end{bmatrix}. \tag{10}$$

Then, a local Cartesian frame (x', y', z') centered on $\Omega \equiv \mathbf{P}$ is introduced in terms of the direction cosine matrix R

$$\begin{bmatrix} x \\ y \\ z \end{bmatrix} = \begin{bmatrix} x_\Omega \\ y_\Omega \\ z_\Omega \end{bmatrix} + R \begin{bmatrix} x' \\ y' \\ z' \end{bmatrix} \tag{11}$$

being

$$\begin{aligned} &\hat{x}' = \bar{a}/|\bar{a}| \\ &\hat{y}' = \hat{x}' \times \hat{x} \quad (\text{if } |\hat{x}' \times \hat{x}| = 0 : \hat{y}' = \hat{x}' \times \hat{y}) \\ &\hat{z}' = \hat{x}' \times \hat{y}'. \end{aligned} \tag{12}$$

In this frame, the motion equations can be expressed as

$$\begin{aligned} &x'(t) = \tfrac{1}{2} a\, t^2 + v_t\, t, \; a = |\bar{a}|, && v_t = \langle \bar{v}_{\text{in}}, \bar{x}' \rangle \\ &y'(t) = v_{ny}\, t, && v_{ny} = \langle \bar{v}_{\text{in}}, \bar{y}' \rangle \\ &z'(t) = v_{nz}\, t, && v_{nz} = \langle \bar{v}_{\text{in}}, \bar{z}' \rangle. \end{aligned} \tag{13}$$

By substituting (9) and (11) in (13), the equations of motion in the local coordinates (ξ, η, ζ), in matrix notation, are

$$\begin{bmatrix} \xi(t) \\ \eta(t) \\ \zeta(t) \end{bmatrix} = J^{-1} R \begin{bmatrix} x'(t) \\ y'(t) \\ z'(t) \end{bmatrix} + J^{-1} \begin{bmatrix} x_\Omega - x_1 \\ y_\Omega - y_1 \\ z_\Omega - z_1 \end{bmatrix}. \tag{14}$$

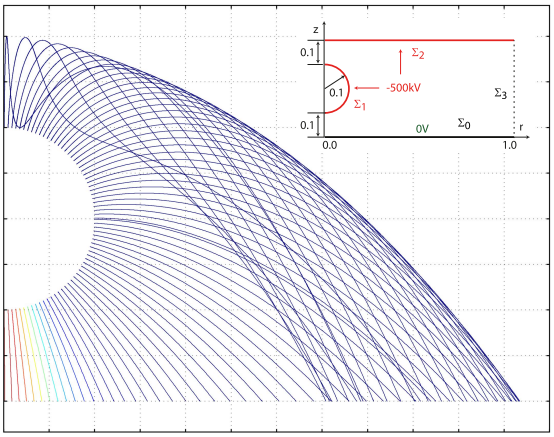

Fig. 3. Sphere–plane configuration: Dirichlet BCs are imposed on $\Sigma_1 \bigcup \Sigma_2$ ($V = -500$ kV), Σ_0 ($V = 0$ V). Neumann BCs on z-axis, Σ_3. Each trajectory is colored as a function of W: the warmer the color, the larger W.

Therefore, **Q** is found by solving (14) with respect to time t, searching for the intersection between the particle trajectory (parabolic curve) and a plane containing a tetrahedron's face:

1) plane 1 (contains nodes 2, 3, and 4): $\xi(t)+\eta(t)+\zeta(t)=1$;
2) plane 2 (contains nodes 1, 3, and 4): $\xi(t) = 0$;
3) plane 3 (contains nodes 1, 2, and 4): $\eta(t) = 0$;
4) plane 4 (contains nodes 1, 2, and 3): $\zeta(t) = 0$.

Then, out of the eight possible solutions $(t_k, k = 1, \ldots, 8)$, the instant in which the particle reaches **Q** is: $t^\star = \min |t_k|$; the Cartesian coordinates (x, y, z) of **Q** can be calculated by substituting $\xi(t^\star)$, $\eta(t^\star)$, $\zeta(t^\star)$ in (9). Finally, by deriving (9) with respect to time t, we obtain the Cartesian components of $\bar{v}_{\text{out}}$

$$\begin{bmatrix} v_x \\ v_y \\ v_z \end{bmatrix} = J \frac{d}{dt} \begin{bmatrix} \xi(t) \\ \eta(t) \\ \zeta(t) \end{bmatrix}_{t=t^\star}. \tag{15}$$

V. Numerical Results

As a preliminary test, the 2-D axisymmetric configuration (sphere–plane) shown in Fig. 3 is considered: Dirichlet BCs are imposed on Σ_0 ($V = 0V$), $\Sigma_1 \bigcup \Sigma_2$ ($V = -500$ kV). Neumann BCs are imposed on z-axis and Σ_3. Particle trajectories are calculated with standard numerical integration of motion equations for 2-D reference solution (fine mesh, second-order elements). Then, the corresponding 3-D configuration is considered; the proposed post-processing tool is applied to the solution calculated by CAFE code ($\approx$250 k tetrahedra). Some representative trajectories from cathode to anode are shown in Fig. 4, together with collections of tetrahedra spanned by the algorithm. A comparison between 3D and 2D solutions is shown in Fig. 5, in terms of couple of values (E_A, electric field and d, distance from z-axis) corresponding to each impact point on Σ_0. An overall good agreement is obtained even for a relatively coarse 3-D mesh. The evaluation of all trajectories ($\approx$2500, with an average number of spanned elements $\mu = 74$) takes less than 30 s on a workstation equipped with two Xeon E5-2680 2.7 GHz for the present MATLAB implementation; a reduction of computation time of at least two orders of magnitude is expected by an efficient OpenMP Fortran implementation.

Then, a complex multi-electrode multi-voltage system is considered (ITER NBI accelerator, Fig. 1). The voltage distribution inside the beam accelerator, calculated by CAFE code, is shown in Fig. 6. Note that, solving the electrostatic problem

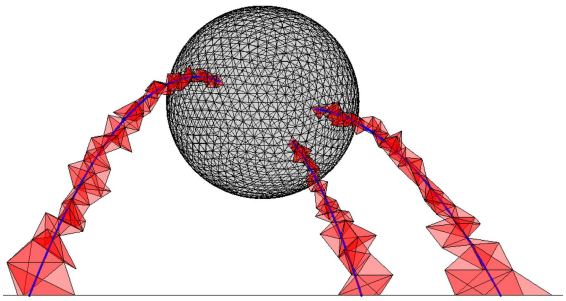

Fig. 4. Sphere–plane configuration: some representative particle trajectories are shown together with tetrahedra spanned by the algorithm applied to the 3-D solution calculated by CAFE code (mesh elements $\approx$ 250 k).

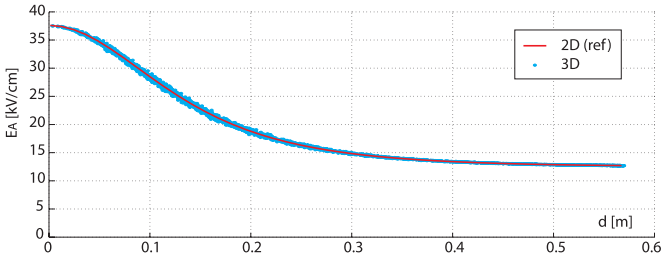

Fig. 5. Sphere–plane configuration: comparison between 3-D and 2-D solutions, in terms of couple of values (E_A, electric field and d, distance from z-axis) corresponding to each impact point on Σ_0.

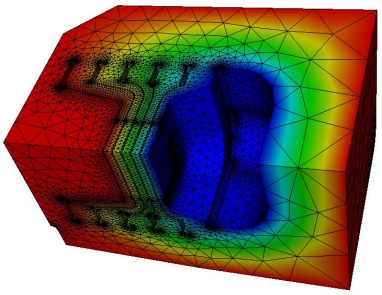

Fig. 6. Voltage distribution inside the beam accelerator calculated by CAFE code. The initial mesh ($\approx$200 k tetrahedra) is superimposed to the solution.

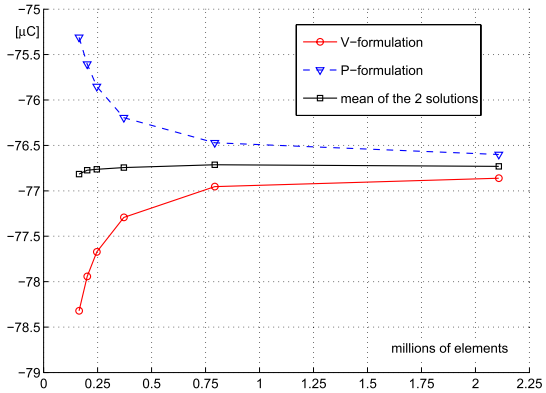

Fig. 7. Study of convergence, in terms of electrostatic charge deposited on the -1 MV electrode. The mean of the two solutions is much more accurate than the solutions provided by each formulation alone.

two times, by employing both complementary formulations (**V**, **P**), does not represent an overhead: the constitutive error is minimized and upper–lower bounds for system energy are given in a rigorous way. Moreover, the mean of the two solutions is usually much more accurate than the solutions provided by each formulation alone, with a strong reduction in the computational cost of the simulation for a given accuracy.

TABLE I
CHARGE DEPOSITED ON EACH ACCELERATING STAGE [μC]. COMPARISON BETWEEN **V** AND **P** FORMULATIONS

	-1MV	-0.8MV	-0.6MV	-0.4MV	-0.2MV	0V
V	-76.9	-4.03	-10.28	-12.61	-0.74	104.5
P	-76.6	-4.05	-10.13	-12.44	-0.62	103.8
mean	-76.7	-4.04	-10.21	-12.53	-0.68	104.2

Fig. 7 shows the results of the study of convergence, in terms of electrostatic charge deposited on -1 MV electrode. It can be observed that the mean of the two solutions is much more accurate than the solutions provided by each formulation alone, and is relatively close to the right value even for the coarsest mesh. After five steps of adaptive refinement, the convergence is almost reached (relative error below 0.3%); the final mesh consists of $\approx$2.1 millions of tetrahedra. Table I summarizes the results of the comparison between **V** and **P** solutions, in terms of electrostatic charge deposited on each electrode, for the final mesh.

VI. CONCLUSION

An innovative approach for the voltage breakdown prediction in high-voltage systems, insulated by large vacuum gaps, has been presented. The breakdown voltage evaluation in terms of probability makes this model suitable for an engineering approach to the insulation design; in particular, the electrode profile design would be no longer based upon the electric field minimization but upon the minimization of the new breakdown driver parameter W.

At this purpose, two complementary formulations of the electrostatic field laws have been developed and implemented in a numerical code (CAFE), together with a post-processing tool based on the analytical solution of motion equations. The two formulations provide a robust error estimator for adaptively refine the mesh and to have a reliable control on the accuracy of the solution.

REFERENCES

[1] N. Pilan, P. Veltri, and A. De Lorenzi, "Voltage holding prediction in multi-electrode multi-voltage systems insulated in vacuum," *IEEE Trans. Dielectr. Electr. Insul.*, vol. 18, no. 2, pp. 553–560, Apr. 2011.

[2] L. Cranberg, "The initiation of the electrical breakdown in vacuum," *J. Appl. Phys.*, vol. 23, no. 5, pp. 518–522, 1952.

[3] I. N. Slivkov, "Mechanism for electrical discharge in vacuum," *Soviet Phys.-Tech. Phys.*, vol. 2, pp. 1928–1934, 1957.

[4] P. Bettini, R. Specogna, and F. Trevisan, "Electroquasistatic analysis of the gas insulated line for the ITER neutral beam injector," *IEEE Trans. Magn.*, vol. 45, no. 3, pp. 996–999, Mar. 2009.

[5] P. Stanley, A. Sivill, and H. Fessler, "Applications of the four function Weibull equation in the design of brittle components," in *Flaws and Testing* (Fracture Mechanics of Ceramics). New York, NY, USA: Plenum, 1978.

[6] A. De Lorenzi, N. Pilan, A. Pesce, and E. Spada, "Validation progresses of the voltage holding prediction model at the high voltage padova test facility hvptf," in *Proc. 25th ISDEIV*, 2012, pp. 9–13.

[7] R. Specogna, "Complementary geometric formulations for electrostatics," *Int. J. Numer. Meth. Eng.*, vol. 86, no. 8, pp. 1041–1068, 2011.

[8] J. Rikabi, C. Bryant, and E. Freeman, "Complementary solutions of electrostatic field problems," *IEEE Trans. Magn.*, vol. 25, no. 6, pp. 4427–4442, Nov. 1989.

[9] R. Specogna, "Optimal cohomology generators for 2-D eddy-current problems in linear time," *IEEE Trans. Magn.*, vol. 49, no. 4, pp. 1299–1304, Apr. 2013.

[10] L. Codecasa, R. Specogna, and F. Trevisan, "Symmetric positive-definite constitutive matrices for discrete eddy-current problems," *IEEE Trans. Magn.*, vol. 43, no. 2, pp. 510–515, Feb. 2007.